

Statistics of Dislocation Slip Avalanches in Nanosized Single Crystals Show Tuned Critical Behavior Predicted by a Simple Mean Field Model

Nir Friedman,¹ Andrew T. Jennings,² Georgios Tsekenis,¹ Ju-Young Kim,³ Molei Tao,⁴ Jonathan T. Uhl,[†]
Julia R. Greer,^{2,5} and Karin A. Dahmen^{1,*}

¹Department of Physics, University of Illinois at Urbana-Champaign, 1110 West Green Street, Urbana, Illinois 61801-3080, USA

²Division of Engineering and Applied Sciences, MC309-81, Caltech, Pasadena, California 91125-8100, USA

³School of Mechanical and Advanced Materials Engineering, Ulsan National Institute of Science and Technology (UNIST),
Ulsan 689-798, Republic of Korea

⁴Department of Computing and Mathematical Sciences, MC305-16, Caltech, Pasadena, California 91125-8100, USA

⁵The Kavli Nanoscience Institute at the California Institute of Technology, Pasadena, California 91125, USA

(Received 6 December 2011; published 30 August 2012)

We show that slowly sheared metallic nanocrystals deform via discrete strain bursts (slips), whose size distributions follow power laws with stress-dependent cutoffs. We show for the first time that plasticity reflects tuned criticality, by collapsing the stress-dependent slip-size distributions onto a predicted scaling function. Both power-law exponents and scaling function agree with mean-field theory predictions. Our study of 7 materials and 2 crystal structures, at various deformation rates, stresses, and crystal sizes down to 75 nm, attests to the universal characteristics of plasticity.

DOI: [10.1103/PhysRevLett.109.095507](https://doi.org/10.1103/PhysRevLett.109.095507)

PACS numbers: 62.25.-g, 61.46.Hk, 81.07.-b, 89.75.-k

Introduction.—Sheared small-scale crystals deform via a sequence of discrete slips, measurable either as steps in stress-strain curves or as acoustic emission pulses [1–13]. We show that the statistical distributions of the slip sizes and their stress dependence (i) reflect *tuned* criticality, (ii) agree with the predictions of a simple mean-field theory (MFT) model, down to 75-nm-diameter samples, and (iii) reflect the same scaling behavior (universality) for a wide variety of materials, crystal structures, size scales, and experimental parameters.

The slips are caused by dislocation slip avalanches resulting from rapid dislocation nucleation or sudden releases of dislocations from pinned sources. They stop when all slipping dislocation segments have either repinned or are annihilated. Recent experiments on the axial compression of micron- and submicron-sized crystals reported that the stress-integrated distributions (histograms) $D_{\text{int}}(S)$ of all slip sizes S (starting from the initiation of compression to pillar failure) follow a power law $D_{\text{int}}(S) \sim S^{-1.5}$ over several decades in S . Here S is the total axial displacement during an avalanche (see Supplemental Material [14]). This has been seen in experiments on micron and submicron pillars of face-centered cubic (fcc) metals (Cu, Al, Au, and Ni) and one body-centered cubic (bcc) metal (Mo) [8,9,15–17]. However, up to now, the slip statistics were far from understood. Here we report three main results that provide a new unified understanding.

(i) *Tuned criticality.*—Previous experimental studies focused on fitting exponents k to power-law distributions $D(S) \sim S^{-k}$, similar to self-organized criticality (SOC) [5,6,8]. SOC assumes that the (“cutoff”) size S_{max} of the largest observed avalanche exclusively depends on the system size and not on other experimental parameters.

However, a simple analytical MFT model [2] and simulations [1] predict that the cutoff S_{max} can also depend on the stress, implying that plasticity reflects tuned criticality. The long-standing fundamental debate of SOC versus tuned criticality so far has remained unresolved for plasticity, due to a lack of experimental evidence of cutoff tunability. Here we show for the first time that for nanocrystals the cutoff size grows as the stress approaches the failure stress (or “critical stress”) τ_c as predicted by MFT and simulations [1,2]. Below the critical stress, a slow stress increase in the material produces microscopically small slip avalanches. Above the critical stress τ_c , the material deforms in a macroscopic slip avalanche until it fails. The model predicts that the critical stress τ_c is a critical point separating these two regimes. (The value of τ_c depends on the details of the system [18–20]). Near τ_c the system shows *universal* (detail-independent) avalanche statistics, as predicted by the theory of phase transitions and the renormalization group [2,19,20]. We extract a predicted scaling collapse of the stress-dependent avalanche-size distributions from the experiments which shows that plasticity indeed reflects the predicted tuned critical point with stress as a tuning parameter. We also show why tuned criticality was not observed before in experiments and how it is reconciled with previous experiments.

(ii) *Agreement with MFT predictions.*—The MFT slip-size distribution depends on stress τ as $D(S, \tau) \sim S^{-\kappa} f_S[S(\tau_c - \tau)^{1/\sigma}]$, where $\kappa = 1.5$, $\sigma = 0.5$, and $f_S(x)$ is an exponentially decaying universal scaling function [2]. Consequently, the largest expected avalanche size $S_{\text{max}}(\tau)$ grows with stress as $S_{\text{max}}(\tau) \sim (\tau_c - \tau)^{-1/\sigma}$. For the first time we extract and collapse the experimental avalanche-size distributions $D(S, \tau)$ from different stress bins. The

scaling-collapse agrees with the MFT predictions for $\kappa = 1.5$, $\sigma = 0.5$, and the scaling *function*, which contains more information than the traditionally fitted power-law exponent κ alone. This collapse thus constitutes a much more stringent test of MFT, confirming that the slip statistics of plasticity indeed reflect the underlying tuned non-equilibrium critical point predicted by MFT [1–3], as explained above. The model also explains our observed dependence of the slip statistics on compression rate and system size.

(iii) *Universality*.—The simple MFT provides a unified understanding of plasticity at nano- and microscales [10–12]. In experiments, at first sight, plasticity looks different on these two scales. At nanoscales the lattice structure matters. For example, the dislocation dynamics and the criticality slope (defined as the slope of the stress-strain curve prior to failure [Fig. 1(c)]), depend on the material’s crystal structure [9–12,18]. Here, we show (a) how MFT relates these features to the slip statistics and (b) that MFT applies to all crystal structures on nano- and microscales, despite the apparent differences observed in experiments.

In summary, we show that MFT provides a unified explanation for plasticity as a tuned critical phenomenon

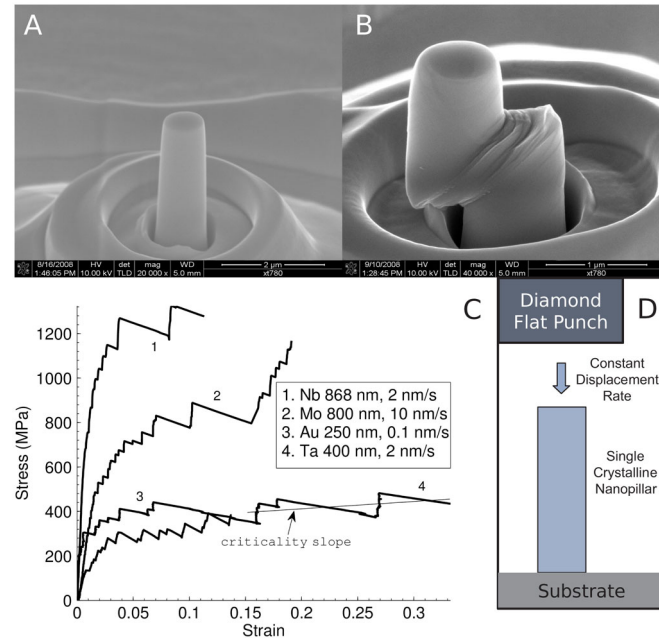


FIG. 1 (color online). Nanopillar compression tests. (a), (b) SEM images of a 868-nm-diameter Nb pillar at 52° tilt, before and after compression, respectively. (b) Pillar after final catastrophic slip event; slip data at the largest strains are excluded from the analysis. (c) Characteristic stress-strain curves (each contains thousands of points) for four metals compressed at different displacement rates. Negatively sloped lines connect two points at the beginning and end of fast slips, with springlike machine response. The Nb stress-strain curve corresponds to the pillar in (a)–(b). The “criticality slope” line is fitted to the average slope of curve 4, near the critical (failure) stress (see the text). (d) Schematic of the compression test methodology. For details, see Supplemental Material [14].

under a wide variety of conditions: for pillar sizes ranging from 75 nm to 1 μm , for strain rates less than or on the order of $1 \times 10^{-4} \text{ s}^{-1}$, for different materials, and for different crystal structures. It predicts the power-law exponents and scaling function of the slip-size distributions and the stress dependence of their cutoffs.

In the following, we first discuss the model predictions and then compare them to stress-integrated and stress-binned (i.e., stress-dependent) slip-size distributions measured during uniaxial compression of nanopillars for different values of stress, deformation rate, and pillar size. The analysis tools and methods [19] applied here to experiments are generally applicable to a much broader set of future experiments on plasticity and slip-avalanche statistics [20,21].

Simple MFT model for slow shear.—Our simple coarse-grained model is described in detail in Ref. [2]. It makes robust statistical predictions for material deformation given the following assumptions: (i) A slowly sheared material has weak spots where slip initiates when the local stress exceeds a random local threshold stress. (ii) Slip avalanches occur at length scales that are large compared with the microscopic structure of the material. (iii) The material is sheared sufficiently slowly so that slip avalanches do not overlap in time. (iv) The MFT approximation replaces the long-range elastic interactions with infinite range interactions.

A failed spot slips until the local stress is reduced to a random arrest stress and then resticks. The stress released by a failed spot triggers other elastically coupled weak spots to slip, creating a slip avalanche. According to assumption (iii), avalanches occur faster than the slow, imposed material deformation. We extract detail-independent (universal) analytical predictions [2], which agree with numerical studies of continuum models [1,22], phase fields [23], phase field crystals [24], discrete 2D dislocation dynamics [1,3,22,25,26], and full 3D dislocation dynamics simulations [27].

At applied stress τ , the model predicts that the stress-dependent (“stress-binned”) distribution $D(S, \tau)$ of slip sizes S follows a power law $S^{-\kappa}$ up to a stress-dependent cutoff size $S_{\text{max}} \sim (\tau_c - \tau)^{-1/\sigma}$ (this is the tunability prediction of MFT) [2]:

$$D(S, \tau) \sim S^{-\kappa} f_S(S(\tau_c - \tau)^{1/\sigma}).$$

Here S is the total displacement during a slip avalanche (see Supplemental Material [14]). The exponents $\kappa = 3/2$ and $1/\sigma = 2$ and the cutoff scaling function $f_S(x)$ are universal [1,2]. In MFT, $f_S(x) = \exp(-Ax)$, where A is a nonuniversal constant [2]. τ_c is again the failure stress, also called critical stress. The stress-binned complementary cumulative distribution function is

$$C(S, \tau) \sim \int_S^\infty D(S', \tau) dS' \sim S^{-(\kappa-1)} g(S(\tau_c - \tau)^{1/\sigma}), \quad (1)$$

where $g(x) \equiv \int_x^\infty e^{-At} t^{-\kappa} dt$ is the universal scaling-function (see Fig. 4, inset). MFT predicts that the stress-integrated histogram $D_{\text{int}}(S)$ of slip sizes follows a power law (see Supplemental Material [14]):

$$D_{\text{int}}(S) \equiv \int D(S, \tau) d\tau \sim S^{-(\kappa+\sigma)} \quad (2)$$

with $\kappa + \sigma = 2$. The stress-integrated complementary cumulative distribution function

$$C(S) \equiv \int_S^\infty D_{\text{int}}(S') dS' \sim S^{-(\kappa+\sigma-1)} \quad (3)$$

then scales as $C(S) \sim S^{-1}$ in MFT (Figs. 2–4). MFT predicts identical power-law exponents for fcc nanopillars (whose stress-strain curves end with the virtually vanishing criticality slopes), as for bcc metals (with a finite, nonzero criticality slope) [2,18]. The above predictions apply to slow compression rates where avalanches are separated in time.

At higher compression rates Ω , avalanches can overlap in time. A general theory [28] predicts that merging of avalanches in time, i.e., activating new avalanches before the previous ones complete, leads to smaller exponent values at higher Ω [28]: At faster compression rates Ω we expect $\kappa + \sigma < 2$, while at slow Ω we expect $\kappa + \sigma = 2$ [Fig. 3 and Eq. (2)].

Compression experiments on single-crystalline nanopillars.—Experimental load and displacement data were obtained from uniaxial compressions of fcc and bcc single-crystalline, cylindrical nanopillars with diameters ranging from 75 to 1000 nm and aspect ratios (height/diameter) between 3:1 and 6:1 (Fig. 1). The experimental procedure (methods section) provided time series of applied load, axial displacement, and slip sizes S for each

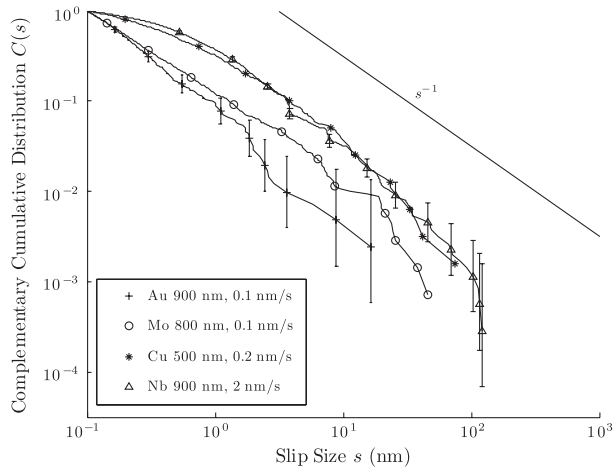


FIG. 2. Stress-integrated cumulative histograms $C(S)$ of slip sizes S (i.e., the fraction of slips with sizes $>S$ plotted versus S) for uniaxial compression of various materials, pillar sizes, and nominal displacement rates, integrated over stress from zero to critical (failure) stress. $C(S)$ contains hundreds of points (one point per event). Error bars [from Bayesian 95% confidence bounds (see Supplemental Material [14])] are shown for histograms with the most and the least points for clarity. Fitted probability density function power-law exponents: 2.1 ± 0.1 (Au), 1.85 ± 0.1 (Mo), 1.8 ± 0.2 (Cu), and 1.9 ± 0.2 (Nb) (subtract 1 for CDF exponents). Fits were obtained from maximum likelihood estimates [32] (see Supplemental Material [14] for error bars and fitting techniques for all figures).

tested pillar. The sampling frequency was 25 Hz, and by noting where the slip distribution changes from power-law to Gaussian we concluded that slip identification was reliable down to events as small as $O(0.3 \text{ nm})$. Au, Nb, Mo, Ta, and W nanopillars were fabricated via focused ion beam methodology [9,16,17], and Cu pillars were created via templated electroplating [29], and were compressed at various displacement rates. For a slowly increasing applied load, the stress remains approximately constant during each slip, as assumed in the model. This applies to all experiments, as the slip speed is much greater than the externally imposed strain rates [30]. The data were collected on two nanoindenters: one with a high stiffness of 300 000 N/m and one with a stiffness of 65 000 N/m; no systematic difference based on machine stiffness was observed.

Figures 2–5, respectively, show experimental stress-integrated and stress-binned complementary cumulative histograms. The major source of error is statistical, caused by small event numbers. Across all tested materials, the cumulative histograms display a power-law regime with an exponent close to the theoretical value of -1 (see Fig. 2). The data in Fig. 2 were collected for large system sizes and at low nominal displacement rates—a regime closest to the scaling regime of the MFT model. These plots show that both fcc and bcc nanocrystals of different diameters and compressed at different displacement rates display the same power-law exponents despite the distinct differences in their dislocation behavior as reported in Refs. [9,18]. The materials show slight differences in how the changing nominal displacement rates affects the statistical data.

Figure 3 shows the results for three different nominal displacement rates, varying by an order of magnitude, for

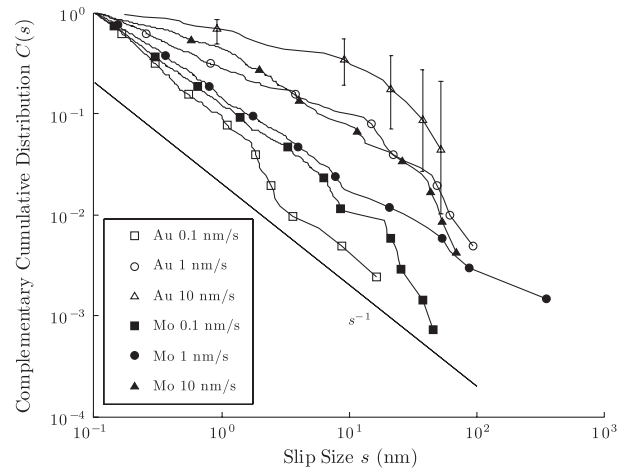


FIG. 3. Stress-integrated cumulative histograms $C(S)$ of slip sizes S for uniaxial compression data: comparison of the impact of nominal displacement rate for Mo and Au pillars of diameter 800 nm. The nominal displacement rate impacts the apparent power laws of the cumulative slip-size histograms. The fitted probability density function exponents are 2.1 ± 0.1 , 1.45 ± 0.1 , 1.2 ± 0.2 , 1.85 ± 0.1 , 1.8 ± 0.1 , and 1.6 ± 0.3 , in the order of the legend (subtract 1 for CDF exponents). The lowest rates are used to compare with model predictions.

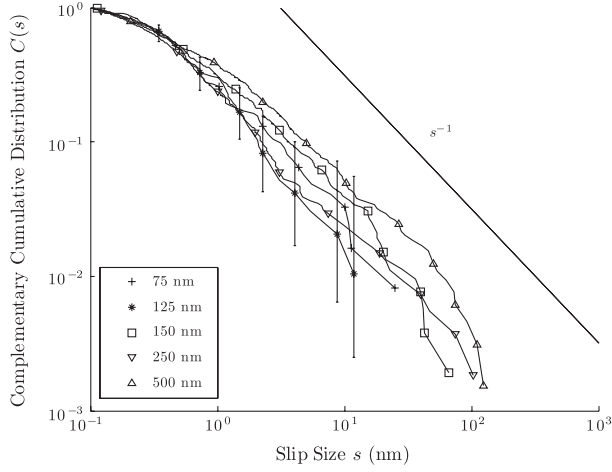


FIG. 4. Stress-integrated cumulative histograms $C(S)$ of the slip size S for various sizes of Cu nanopillars compressed at a displacement rate of 2 nm/s. Larger pillars have larger maximum slip events, except for the 125 nm pillars, for which less data were taken. (For power-law distributions, the largest expected slip size increases with the total number of slips.)

800-nm-diameter Au and Mo pillars. The avalanche-size distribution for Mo is fairly robust from 0.1 to 1 nm/s, but the magnitude of the fitted scaling exponent of $C(S)$ decreases at 10 nm/s. Au is much more sensitive to the prescribed displacement rate: The magnitude of the scaling exponent of $C(S)$ again decreases with the increasing displacement rate. As discussed in the theory section and in Ref. [28], at higher driving rates avalanches can overlap in time, thereby reducing the scaling exponents of $C(S)$. Note that limited time resolution may also cause avalanches to appear as overlapping in time. Theory predicts that the amounts by which the exponents change as the displacement rate is increased depend on the material [28], as corroborated by our experiments. The results of Fig. 3 for different nominal displacement rates are thus consistent with the theories of Refs. [2,28].

We also considered the impact of system size on the slip-size distributions. Sufficiently close to the critical (failure) stress, the correlation length reaches the system size. Consequently, the pillar diameter projected onto a shear slip plane determines the scale of the largest slip events and, hence, the cutoff of the stress-integrated slip-size distribution. Figure 4 shows $C(S)$ for Cu, for various nanopillar sizes compressed at the same displacement rate of 2 nm/s. Although events are few and statistical fluctuations pronounced, the trend of increasing maximum avalanche size with system size is visible in Fig. 4.

Figure 5 shows that the cumulative slip-size histograms binned in stress also agree with the model's prediction for $C(S, \tau)$ of Eq. (1) (see Supplemental Material [14]). The main figure shows data from four distinct stress bins, while the inset shows a data collapse using the exponents $\kappa - 1 = 0.5$ and $1/\sigma = 2$ predicted by MFT. Stress bins closer to the critical stress than those shown were not used in the collapse, in order to avoid finite size effects (since

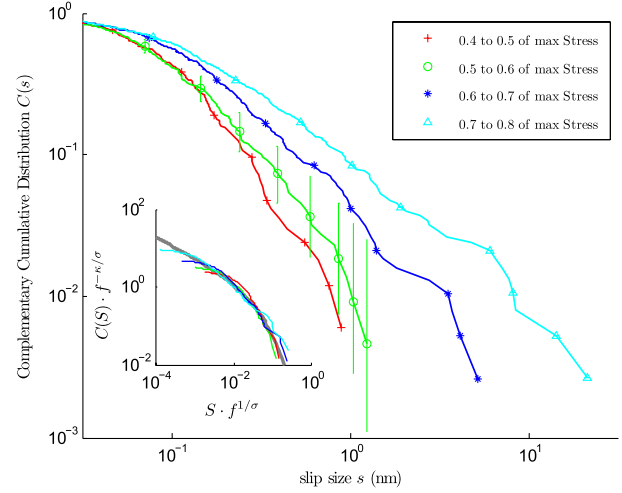


FIG. 5 (color online). Main figure: Stress-binned cumulative histogram $C(S, \tau)$ of slip sizes S as a function of applied stress τ , using events from 7 Mo nanopillars, of approximate diameter 800 nm, compressed at 0.1 nm/s nominal displacement rate. The events from each pillar are normalized according to their respective maximum stress. Inset: Scaling collapse of the same data, $f = (\tau_c - \tau)/\tau_c - c'$, where $c' = 0.14$ is an adjustable parameter that compensates for finite system size (see Supplemental Material [14]); $\kappa = 1.5$ and $1/\sigma = 2$ (as predicted by MFT), and the gray function is the predicted MFT scaling function, $g(x) = \int_x^\infty e^{-At} t^{-\kappa} dt$.

near the critical stress, the correlation length is capped by the system size; see Supplemental Material [14]). The inset shows that the theoretically predicted collapse function (continuous gray line) falls on top of the experimental collapse. This reveals that MFT not only predicts the exponents used for the successful collapse but also predicts the scaling function [2]. This constitutes the first experimental validation of a universal scaling function predicted by the simple MFT model. The collapse also confirms the stress-integrated power law of -1 for $C(S)$ seen in Figs. 2–4.

Discussion.—Recent uniaxial deformation experiments and simulations provide insight into the physical nature of dislocation sources, size dependence of material strength, strain rate sensitivity, and amount of hardening [10–12]. The consensus is that these factors vary greatly between fcc and bcc crystals and from nano- to microscale. The question emerges whether these differences are also manifested by the dislocation slip statistics. Our experiments yield a stress-integrated exponent of $\kappa + \sigma = 2$ for the slip-size distributions, for both bcc and fcc nanopillars with diameters between 75 nm and 1 μm , in agreement with the MFT prediction. In contrast, previous experiments on Mo and Au [9,15] have reported a size-distribution exponent of 1.5 for samples ranging in size from 180 nm to 6 μm . Our model provides a unified understanding of the statistics in all these cases: (i) The compression experiments of Ref. [15] on submicron samples were performed at higher effective compression rates (Fig. 3), where lower exponents can be explained by the merging of slip avalanches [28]. We

observed significant impact on the exponent for rates as slow as 1 nm/s. (ii) Many micron-sized samples display a large regime before failure where the stress-strain curve is linear due to hardening [8,11]. Such behavior can be captured by modifying the MFT model to include hardening through incorporating an increased resistance to slip during deformation. In this case, the effective stress distance from criticality remains constant [1], and the experiment effectively measures κ rather than $\kappa + \sigma$. In this case the SOC assumption [5,6,8] with the measured value of $\kappa = 1.5$ is valid and agrees with the MFT predictions [1,2,27,31].

In conclusion, this study presents the first scaling collapse and scaling function extracted from compression experiments on nanopillars and micropillars. It shows that plasticity is a tuned critical phenomenon. Both the exponents and the scaling function of the stress-dependent strain-burst statistics agree with predictions from a simple analytical MFT model. This agreement constitutes the most stringent test of the MFT model and tuned criticality to date, since scaling functions contain much more information than the traditional sets of exponents. The agreement between the MFT model and experiments for a wide variety of metallic nanocrystals subjected to widely varying experimental conditions suggests that a single universality class fully describes discrete crystalline deformation at these small length scales. This holds true under a wide variety of conditions: for pillar sizes ranging from 75 nm to 1 μm , for strain rates less than or on the order of $1 \times 10^{-4} \text{ s}^{-1}$, and for different materials including those with fcc and bcc crystal structures. This agreement is observed both in the power-law scaling of the event frequency as well as in the stress dependence of the slip-size distributions. This robustness indicates that these analysis methods are broadly applicable to other nonequilibrium systems with driving-force-dependent avalanches [20]. In the context of the renormalization group [2,19,20] our results imply that the same fundamental properties—symmetries, dimensions, interaction range, etc.—control the statistics of slips in metallic crystals, down to the smallest currently accessible length scales.

We thank James Antonaglia, Braden Brinkman, Dennis Dimiduk, Tyler Earnest, Robert Maass, and Matthew Wraith for helpful conversations and acknowledge the financial support of NSERC (N.F.) and from grants NSF No. DMR 03-25939 ITR (“Materials Computation Center”) and No. DMR 1005209 (G.T. and K.D.), as well as from NSF (A.T.J.), NSF CAREER Grant No. DMR-0748267 (J.R.G.), and ONR Grant No. N00014-09-1-0883 (J.R.G.). K.D. also thanks the Kavli Institute of Theoretical Physics at UC Santa Barbara for hospitality and support.

*To whom correspondence should be addressed.

dahmen@illinois.edu

†Retired.

[1] M. Zaiser, *Adv. Phys.* **55**, 185 (2006).

- [2] K. A. Dahmen, Y. Ben-Zion, and J. T. Uhl, *Phys. Rev. Lett.* **102**, 175501 (2009).
- [3] M.-C. Miguel, A. Vespignani, S. Zapperi, J. Weiss, and J. R. Grasso, *Nature (London)* **410**, 667 (2001).
- [4] J. Weiss, J. R. Grasso, M.-C. Miguel, A. Vespignani, and S. Zapperi, *Mater. Sci. Eng. A* **309–310**, 360 (2001).
- [5] T. Richeton, P. Dobron, F. Chmelik, J. Weiss, and F. Louchet, *Mater. Sci. Eng. A* **424**, 190 (2006).
- [6] T. Richeton, J. Weiss, and F. Louchet, *Acta Mater.* **53**, 4463 (2005).
- [7] J. Weiss, F. Lahaie, and J. R. Grasso, *J. Geophys. Res.* **105**, 433 (2000).
- [8] D. M. Dimiduk, C. Woodward, R. LeSar, and M. D. Uchic, *Science* **312**, 1188 (2006).
- [9] S. Brinckmann, J.-Y. Kim, and J. R. Greer, *Phys. Rev. Lett.* **100**, 155502 (2008).
- [10] J. R. Greer and J. T. M. De Hosson, *Prog. Mater. Sci.* **56**, 654 (2011).
- [11] M. D. Uchic, P. Shade, and D. Dimiduk, *Annu. Rev. Mater. Res.* **39**, 361 (2009), and references therein.
- [12] O. Kraft, P. Gruber, R. Mönig, and D. Weygand, *Annu. Rev. Mater. Res.* **40**, 293 (2010), and references therein.
- [13] A. H. W. Ngan and K. S. Ng, *Philos. Mag.* **90**, 1937 (2010).
- [14] See Supplemental Material at <http://link.aps.org/supplemental/10.1103/PhysRevLett.109.095507> for additional information on the technical details of both the analysis and the experiment.
- [15] M. Zaiser, J. Schwerdtfeger, A. S. Schneider, C. P. Frick, B. G. Clark, P. A. Gruber, and E. Arzt, *Philos. Mag.* **88**, 3861 (2008).
- [16] J.-Y. Kim and J. R. Greer, *Acta Mater.* **57**, 5245 (2009).
- [17] J.-Y. Kim, D. Jang, and J. R. Greer, *Acta Mater.* **58**, 2355 (2010).
- [18] C. R. Weinberger and W. Cai, *Proc. Natl. Acad. Sci. U.S.A.* **105**, 14304 (2008).
- [19] N. D. Goldenfeld, *Lectures on Phase Transitions and the Renormalization Group* (Westview, Boulder, CO, 1992).
- [20] J. P. Sethna, K. A. Dahmen, and C. R. Myers, *Nature (London)* **410**, 242 (2001).
- [21] A. P. Mehta, A. C. Mills, K. A. Dahmen, and J. P. Sethna, *Phys. Rev. E* **65**, 046139 (2002).
- [22] M. Zaiser, in *Statistical Mechanics of Plasticity and Related Instabilities*, provided by the SAO/NASA Astrophysics Data System (2005).
- [23] M. Koslowski, *Philos. Mag.* **87**, 1175 (2007).
- [24] P. Y. Chan, G. Tsekenis, J. Dantzig, K. A. Dahmen, and N. Goldenfeld, *Phys. Rev. Lett.* **105**, 015502 (2010).
- [25] G. Tsekenis, N. Goldenfeld, and K. A. Dahmen, *Phys. Rev. Lett.* **106**, 105501 (2011).
- [26] P. D. Ispanovity, I. Groma, G. Gyorgyi, F. F. Csikor, and D. Weygand, *Phys. Rev. Lett.* **105**, 085503 (2010).
- [27] F. F. Csikor, C. Motz, D. Weygand, M. Zaiser, and S. Zapperi, *Science* **318**, 251 (2007).
- [28] R. A. White and K. A. Dahmen, *Phys. Rev. Lett.* **91**, 085702 (2003).
- [29] A. T. Jennings, M. J. Burek, and J. R. Greer, *Phys. Rev. Lett.* **104**, 135503 (2010).
- [30] A. T. Jennings, J. Li, and J. R. Greer, *Acta Mater.* **59**, 5627 (2011).
- [31] G. Tsekenis, J. T. Uhl, N. Goldenfeld, and K. A. Dahmen (to be published).
- [32] M. E. J. Newman, *Contemp. Phys.* **46**, 323 (2005).